OPEN ACCESS

Japanese Journal of Applied Physics **61**, 078002 (2022) **BRIEF NOTE**

https://doi.org/**10.35848/1347-4065/ac74fe**

Strain-insensitive high-sensitivity temperature sensing based on multimode interference in a square-core fiber

Kun Wang[1*], Yosuke Mizuno[2], Xingchen Dong[1], Wolfgang Kurz[1], Maximilian Fink[1], Martin Jakobi[1], and Alexander W. Koch[1]

[1]*Institute for Measurement Systems and Sensor Technology, Department of Electrical and Computer Engineering, Technical University of Munich, Arcisstraβe 21, Munich 80333, Germany*

[2]*Faculty of Engineering, Yokohama National University, Yokohama 240-8501, Japan*

[*]E-mail: kun88.wang@tum.de

Received April 25, 2022; revised May 6, 2022; accepted May 30, 2022; published online June 21, 2022

A strain-insensitive high-sensitivity temperature sensor based on multimode interference in a specialty fiber with a square core is developed and experimentally investigated. A 25 cm long square-core fiber is used as a multimode fiber (MMF) of a single-mode–multimode–single-mode structure and the temperature dependence of its transmitted spectrum is measured while the strain is applied continually from 0 to 500 $\mu\varepsilon$ with steps of 100 $\mu\varepsilon$. The mean temperature sensitivity is -22.35 pm °C^{-1}, which is ~3.5 times higher than that of a standard MMF, and it is almost independent of strain with a small standard deviation of 0.44 pm °C^{-1}. © 2022 The Author(s). Published on behalf of The Japan Society of Applied Physics by IOP Publishing Ltd

Optical fiber sensors have been extensively used for several decades due to their intrinsic characteristics, such as compact size, fast response, low cost, and durability against harsh environments.[1–5] One of the most common applications is temperature sensing, and various configurations have been reported including fiber Bragg gratings (FBGs),[6,7] long-period gratings (LPGs),[8,9] Raman scattering,[10] and Brillouin scattering.[11,12] Another type of fiber-optic temperature sensor is based on the inline interference between guided modes in the fiber, which includes Mach–Zehnder interferometry (MZI),[13] Fabry–Perot interferometry (FPI),[14] and Sagnac interferometry.[15] This type of sensor also includes multimode interferometry, which is often implemented using a so-called single-mode–multimode–single-mode fiber (SMS) structure.[16] Here, we focus on the SMS-based temperature sensors.

Although numerous kinds of SMS temperature sensors have been reported, they generally suffer from the crosstalk of different parameters of interest, such as strain. One method to solve this problem is the simultaneous measurement of temperature and strain. For example, an FBG is written in the multimode fiber (MMF) section of an SMS structure to realize an FBG-in-SMS as a multi-parameter sensing module, which is used to measure temperature and strain simultaneously.[17] Oliveira et al. demonstrated a combination of two FBGs written in a standard single-mode fiber, one in an untapered region and the other in a tapered region, spliced to a no-core fiber, which can realize the simultaneous measurement of temperature, strain, and refractive index.[18] Sun et al. reported a fiber sensor by inducing higher-order modal interference based on the SMS structure using a twisted MMF to measure temperature and strain simultaneously.[19] Thus, the demodulation of temperature and strain can be achieved by simultaneous measurement, but it usually requires complicated fabrication.

Another solution is to use a strain-insensitive fiber sensor to measure temperature. Cao et al. investigated a strain-insensitive high-temperature fiber sensor composed of a segment of a small-core photosensitive fiber sandwiched between two single-mode fibers (SMFs).[20] For this purpose, Yao et al. also reported an SMS-based sensor with a few-mode dual-concentric-core fiber (FM-DCCF).[21] Later, Liu et al. proposed a strain-insensitive twist and temperature sensor based on Mach–Zehnder interferometry by a single-mode–multimode–seven-core fiber–multimode–single-mode structure.[22] In addition, Mizuno et al. studied the temperature and strain dependences of the interference spectrum in a hetero-core-fiber structure, which indicates that the hetero-core-fiber-based SMS sensor may enable high-sensitivity temperature measurement with low strain sensitivity.[23]

In this work, based on the conclusion of our previous work[24] that the strain sensitivity at room temperature in an SMS-based sensor using a square-core fiber (SCF) can be extremely low, we demonstrate strain-insensitive temperature sensing by using the SCF-based SMS structure. We investigate the temperature dependence of the transmitted spectral dip while a strain is applied from 0 to 500 $\mu\varepsilon$ with steps of 100 $\mu\varepsilon$. The result shows that the temperature dependence is almost independent of the applied strain and that the mean temperature sensitivity is -22.35 pm °C^{-1} with a standard deviation of as small as 0.44 pm °C^{-1}. The absolute value of this sensitivity is approximately 3.5 times larger than that with a standard MMF-based SMS sensor,[25] which indicates that strain-insensitive high-sensitivity temperature sensing is feasible with the SCF-based SMS sensor.

The sensor configuration consists of a section of an SCF sandwiched between two SMFs. The sensing principle of the SMS sensor is based on multimode interference (MMI). When light is guided through the input SMF and injected into the multimode SCF, multiple modes are excited and travel along the SCF with their own propagation constants.[26] At the second conjunction of SCF/SMF, these fields are coupled back to the fundamental mode of the output SMF. Under the assumption that the SCF and the two SMFs are perfectly aligned, according to the detailed calculation,[27,28] the power in the output SMF P_{out} can be given as

$$P_{\mathrm{out}} = |A_0^2 + A_1^2 e^{i(\beta_0-\beta_1)L} + A_2^2 e^{i(\beta_0-\beta_2)L} + \ldots|^2, \quad (1)$$

where A_i is the field amplitude of the ith mode at the first SMF/SCF boundary, β_i is the propagation constant of the ith mode, and L is the length of the SCF. It is clear that P_{out} is

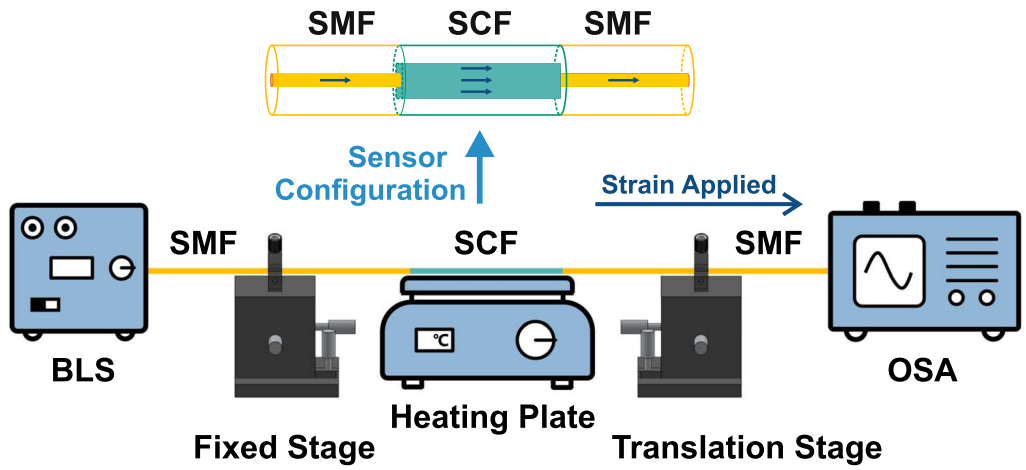

Fig. 1. (Color online) Schematic diagram of the experimental setup and the sensor configuration. BLS, broadband light source; SMF, single-mode fiber; SCF, square-core fiber; OSA, optical spectrum analyzer.

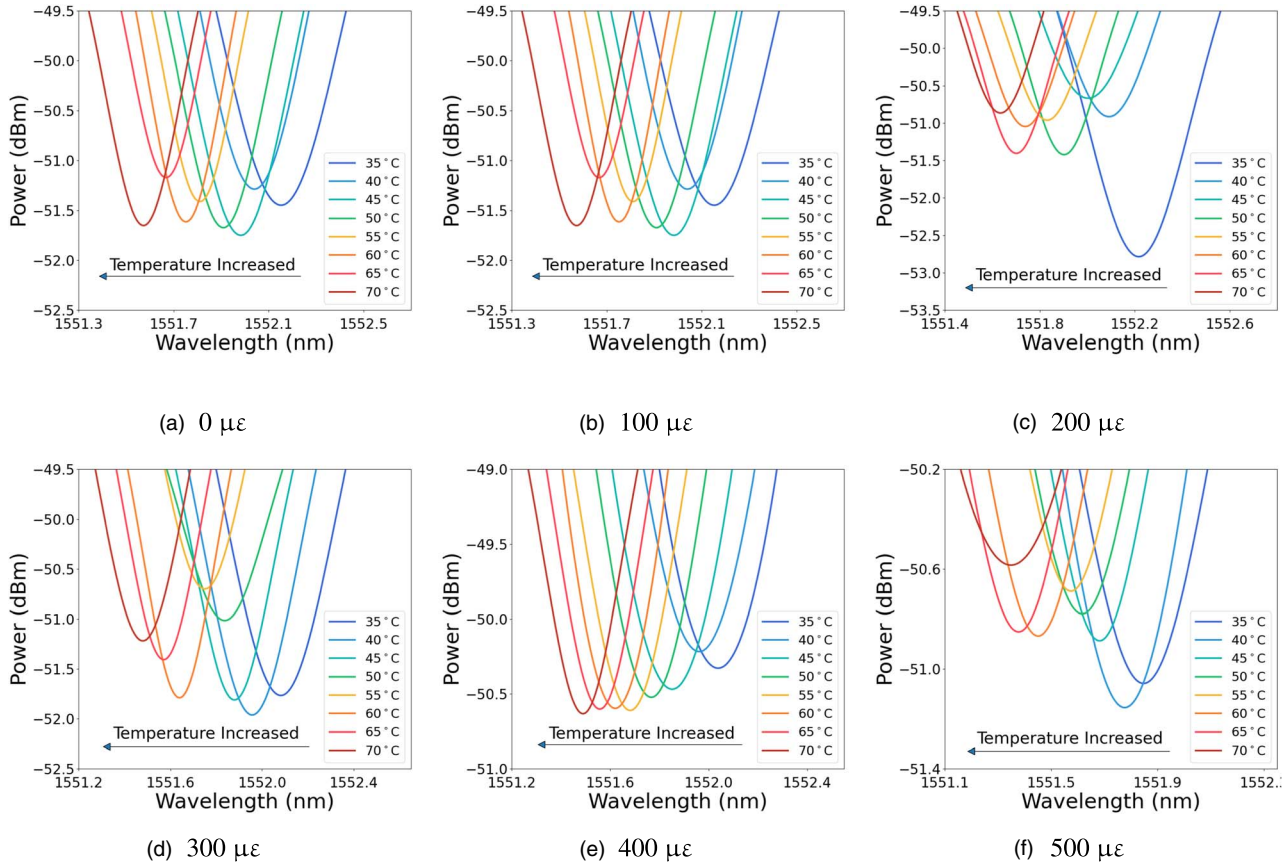

Fig. 2. (Color online) Temperature measurement results with varied applied strains. Measured spectral dependences on temperature: (a) 0 $\mu\varepsilon$, (b) 100 $\mu\varepsilon$, (c) 200 $\mu\varepsilon$, (d) 300 $\mu\varepsilon$, (e) 400 $\mu\varepsilon$, and (f) 500 $\mu\varepsilon$ strains applied.

affected by temperature and strain applied to the SCF, influencing β_i and L. Therefore, temperature and strain sensing can be performed by measuring the shifts in terms of either power or spectral location of dips (or peaks).

The schematic diagram of the experimental setup is shown in Fig. 1. A 25 cm long SCF (FP150QMT, Thorlabs) is connected to two silica SMFs (size: 9/125 μm) by butt-coupling[29] as the sensor head; i.e. both ends of the SCF are connected to the ends of SMFs via FC/PC mating adaptors. The other end of the input SMF is connected to a broadband light source (BLS, central wavelength: 1550 nm) emitting the incident light, while the other end of the output SMF is connected to an optical spectrum analyzer (OSA), which detects the changes in the light spectrum. The SCF section is placed on a heating plate and clamped on two precision translation stages, which are used to apply axial tensile stress on the sensor. The applied axial strain can be calculated by[30]

$$\varepsilon = \frac{\Delta L}{L}, \tag{2}$$

where L is the initial length and ΔL is the additional change in length of the SCF section when the longitudinal stress is applied.

First, the temperature measurement is performed in the range of 35 °C–70 °C in steps of 5 °C with no strain applied. Then, the experiment is carried out under the same condition while the strain is applied in the range of 0–500 $\mu\varepsilon$ with steps of 100 $\mu\varepsilon$. The measured dependences of the spectral dip on temperature are shown in Figs. 2(a)–2(f). The spectral dips exhibit blueshifts in the wavelength domain when the temperature increases. The corresponding resulting wavelength shifts of the spectral dips against the increasing temperature are plotted and fitted in Figs. 3(a)–3(f). The temperature sensitivities are calculated to be −22.19 pm °C^{-1}, −22.19 pm °C^{-1}, −22.79 pm °C^{-1}, −23.01 pm °C^{-1}, −21.96 pm °C^{-1}, and −21.93 pm °C^{-1} for 0 $\mu\varepsilon$, 100 $\mu\varepsilon$, 200 $\mu\varepsilon$, 300 $\mu\varepsilon$, 400 $\mu\varepsilon$, and 500 $\mu\varepsilon$ strain applied. The fitting results are all with high linear regression coefficient (R^2) values in the range of 0.983–0.996.

Figure 4 shows the temperature sensitivities plotted as a function of strain, which is distributed within ± 3% of their mean value of −22.35 pm °C^{-1}. The standard deviation is as small as 0.44 pm °C^{-1}. Our previous work demonstrated the temperature sensitivity of the strain-insensitive temperature sensor using a standard MMF with the same length (25 cm) is 6.32 pm °C^{-1}.[25] Therefore, the absolute value of the temperature sensitivity of the SCF-based sensor is ∼3.5 times that of a standard MMF. This result indicates that the temperature sensitivity exhibits remarkable stability with almost no influence of strain.

In conclusion, we developed a strain-insensitive high-sensitivity temperature sensor based on an SMS structure consisting of a section of an SCF. The obtained mean temperature sensitivity is −22.35 pm °C^{-1}, which is ∼3.5 times higher than the sensitivity (absolute value) of a standard MMF-based configuration under the same condition. And the corresponding standard deviation is 0.44 pm °C^{-1}, which is almost equivalent to the value of using a standard silica fiber. We believe that this work will contribute to the design of strain-insensitive temperature

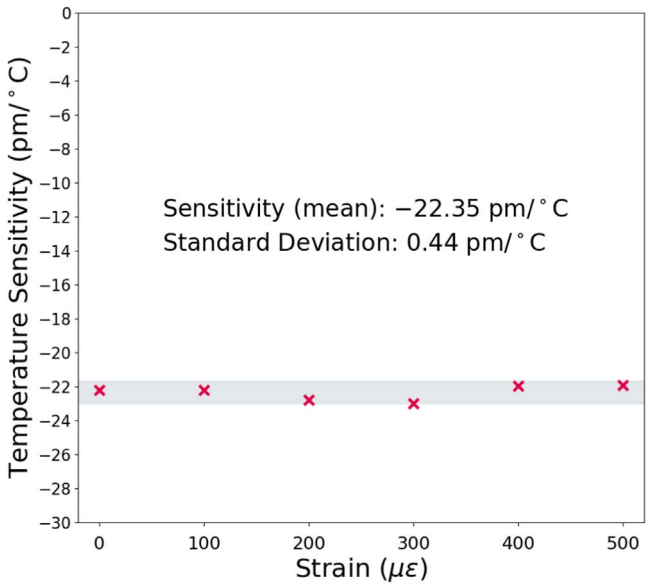

Fig. 4. (Color online) Measured temperature sensitivity plotted as a function of strain. The gray area indicates the ±3% range of the mean temperature sensitivity.

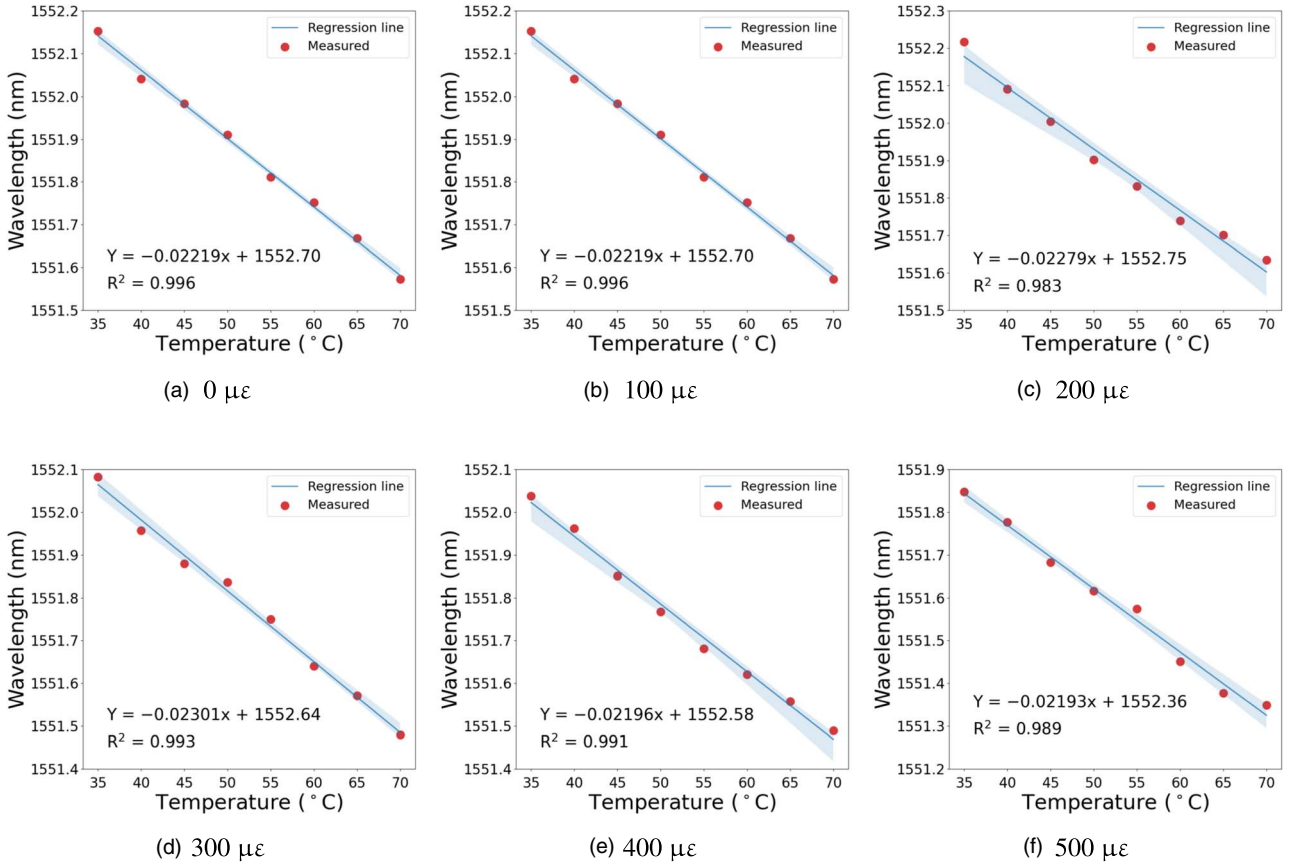

Fig. 3. (Color online) Spectral dip shifts as a function of temperature with varied strains applied: (a) 0 $\mu\varepsilon$, (b) 100 $\mu\varepsilon$, (c) 200 $\mu\varepsilon$, (d) 300 $\mu\varepsilon$, (e) 400 $\mu\varepsilon$, and (f) 500 $\mu\varepsilon$ strains applied.

fiber sensors and also to the development of MMI-based specialty fiber sensors in the future.

Acknowledgments The authors would like to thank the China Scholarship Council (CSC) (Grant No. 201808340074) for supporting this work. Y. M. is indebted to the Japan Society for the Promotion of Science (JSPS) KAKENHI (Grant No. 21H04555), and the research grants from the Murata Science Foundation, the Telecommunications Advancement Foundation, the Takahashi Industrial and Economic Research Foundation, the Yazaki Memorial Foundation for Science and Technology, and the Konica Minolta Science and Technology Foundation.

ORCID iDs Kun Wang https://orcid.org/0000-0003-0410-204X Yosuke Mizuno https://orcid.org/0000-0002-3362-4720

1) X. Wang and O. S. Wolfbeis, Anal. Chem. **92**, 397 (2020).
2) A. Leung, P. M. Shankar, and R. Mutharasan, Sens. Actuators B **125**, 688 (2007).
3) Y. Mizuno, G. Numata, T. Kawa, H. Lee, N. Hayashi, and K. Nakamura, IEICE Trans. Electron. **E101.C**, 602 (2018).
4) K. Wang, X. Dong, M. H. Köhler, P. Kienle, Q. Bian, M. Jakobi, and A. W. Koch, IEEE Sens. J. **21**, 132 (2021).
5) S. Pevec and D. Donlagić, Opt. Eng. **58**, 1 (2019).
6) K. O. Hill and G. Meltz, J. Lightwave Technol. **15**, 1263 (1997).
7) R. Ishikawa, H. Lee, A. Lacraz, A. Theodosiou, K. Kalli, Y. Mizuno, and K. Nakamura, Jpn. J. Appl. Phys. **57**, 038002 (2018).
8) Y. Wang, J. Appl. Phys. **108**, 081101 (2010).
9) C.-L. Zhao, L. Xiao, J. Ju, M. S. Demokan, and W. Jin, J. Lightwave Technol. **26**, 220 (2007).
10) M. N. Alahbabi, Y. T. Cho, and T. P. Newson, Opt. Lett. **30**, 1276 (2005).
11) Y. Mizuno, N. Hayashi, H. Fukuda, K. Y. Song, and K. Nakamura, Light: Sci. Appl. **5**, e16184 (2016).
12) A. Kobyakov, M. Sauer, and D. Chowdhury, Adv. Opt. Photonics **2**, 1 (2010).
13) X. Zhan et al., Opt. Express **26**, 15332 (2018).
14) B. Yin, M. Wang, S. Wu, Y. Tang, S. Feng, and H. Zhang, Opt. Express **25**, 14106 (2017).
15) J. Ruan, P. Huang, Z. Qin, and Q. Zeng, IEEE Photonics Technol. Lett. **27**, 62 (2014).
16) A. Mehta, W. Mohammed, and E. G. Johnson, IEEE Photonics Technol. Lett. **15**, 1129 (2003).
17) D. Song, Q. Chai, Y. Liu, Y. Jiang, J. Zhang, W. Sun, L. Yuan, J. Canning, and G.-D. Peng, Meas. Sci. Technol. **25**, 055205 (2014).
18) R. Oliveira, J. H. Osório, S. Aristilde, L. Bilro, R. N. Nogueira, and C. M. B. Cordeiro, Meas. Sci. Technol. **27**, 075107 (2016).
19) Y. Sun, D. Liu, P. Lu, Q. Sun, W. Yang, S. Wang, L. Liu, and J. Zhang, IEEE Sens. J. **17**, 3045 (2017).
20) Z. Cao, Z. Zhang, X. Ji, T. Shui, R. Wang, C. Yin, S. Zhen, L. Lu, and B. Yu, Opt. Fiber Technol. **20**, 24 (2014).
21) S. Yao, Y. Shen, Y. Wu, W. Jin, and S. Jian, Opt. Laser Technol. **111**, 95 (2019).
22) C. Liu, Y. Jiang, B. Du, T. Wang, D. Feng, B. Jiang, and D. Yang, Sens. Actuator A **290**, 172 (2019).
23) Y. Mizuno, S. Hagiwara, H. Lee, N. Hayashi, M. Nishiyama, K. Wanatabe, and K. Nakamura, Jpn. J. Appl. Phys. **59**, 058002 (2020).
24) K. Wang, X. Dong, P. Kienle, M. Fink, W. Kurz, M. H. Köhler, M. Jakobi, and A. W. Koch, Micromachines **12**, 1239 (2021).
25) K. Wang, Y. Mizuno, X. Dong, W. Kurz, M. Fink, H. Lee, M. Jakobi, and A. W. Koch, arXiv:2204.11044.
26) W. S. Mohammed., P. W. E. Smith, and X. Gu, Opt. Lett. **31**, 2547 (2006).
27) A. Kumar, R. K. Varshney, S. A. C, and P. Sharma, Opt. Commun. **219**, 215 (2003).
28) S. M. Tripathi, A. Kumar, R. K. Varshney, Y. B. P. Kumar, E. Marin, and J.-P. Meunier, J. Lightwave Technol. **27**, 2348 (2009).
29) Y. Mizuno and K. Nakamura, Appl. Phys. Lett. **97**, 021103 (2010).
30) E. Li, Opt. Lett. **32**, 2064 (2007).